https://doi.org/10.31351/vol33iss(4SI)pp101-110

Molecular Modeling, Synthesis, and Preliminary Cytotoxic Activity of New Triazole-Based Derivatives as Expected HDAC Inhibitors

Zaid Mahmood Mohammed[1] and Ayad A. Al-Hamashi[*,2]

[1]Ministry of Health, Babylon Health Directorate, Babylon, Iraq
[2]Department of Pharmaceutical Chemistry, College of Pharmacy, University of Baghdad, Baghdad, Iraq.
***Corresponding Author.**

Received 19/3/2024, Accepted 27/6/2024, Published 15/2/2025

Abstract

Targeting histone deacetylase enzymes (HDACs) is an effective way to treat a variety of diseases, including cancer. Most of the clinically used HDAC inhibitors (HDACis) are pan-inhibitors and have poor pharmacokinetic properties. Therefore, several attempts are ongoing to develop new HDACis with optimum structural features to overcome the structural limitations. In this work, six new triazole-based compounds **K1-K6** were proposed via special modification of common pharmacophores of HDACi using 1,2,4-triazole as a zinc-binding group (ZBG), diverse group in CAP group, and hydrophobic linker. These compounds were analyzed by docking studies against HDAC6, HDAC2, and HDAC8. The docking studies revealed that the proposed compounds have docking scores of **K1** [(*E*)-4-((thiazol-2-ylimino)methyl)-N-(1H-1,2,4- triazol-3-yl)benzamide (-8.54 Kcal/mol)], **K2** [(*E*)-4-((phenylimino)methyl)-N-(1H-1,2,4- triazol-3-yl)benzamide (-8.47 Kcal/mol)], **K3** [(*E*)-4-((p-tolylimino)methyl)-N-(1H-1,2,4- triazol-3-yl)benzamide (-8.46 Kcal/mol)], **K4** [(*E*)-4-((naphthalen-2-ylimino)methyl)-N-(1H-1,2,4- triazol-3-yl)benzamide (-8.32 Kcal/mol)], **K5** [(*E*)-4-(((4-bromophenyl)imino)methyl)-N-(1H-1,2,4- triazol-3-yl)benzamide (-7.62 Kcal/mol)], **K6** [(*E*)-4-(((4-methoxyphenyl)imino)methyl)-N-(1H-1,2,4- triazol-3-yl)benzamide (-6.77 Kcal/mol)], and vorinostat (-9.1 Kcal/mol) against HDAC8. The final compounds were synthesized using conventional organic synthesis methods starting from amide bond formation using the coupling reagents EDCi, DMAP, HOBt, and DIPEA, followed by a Schiff base reaction between the produced aldehyde and various amines to afford the final compounds. The chemical structure for the intermediate and final compounds was characterized using IR and NMR spectroscopies. The preliminary MTT assay of compounds **K1**, **K2**, and **K5** showed a comparable antiproliferative activity with vorinostat against HeLa cells with IC_{50} values for compound **K1** (4.9 µM), **K2** (5.3 µM) and **K5** (5.3 µM) while IC_{50} for vorinostat was (8.4 µM). Most interestingly, compound **K5** showed a higher antiproliferative activity against A549 lung cancer cells with an IC_{50} value (4.4 µM) in comparison to vorinostat (9.5 µM), while compounds **K1**, **K2**, and **K6** have lower cytotoxic effects with IC_{50} of (19.2, 17.6, and 10.6 µM), respectively.
Keywords: HDAC inhibitor, Vorinostat, Molecular docking, MD simulation, Antiproliferative activity.

Introduction

Cancer is a disease characterized by uncontrolled cell proliferation that might invade other body parts[(1)]. Epigenetics refers to a genomic mechanism that modifies gene expression reversibly without changing DNA sequences. There is a strong correlation between epigenetic dysfunctions and cancer. Epigenetic alterations are classified into four distinct mechanisms: DNA methylation, noncoding RNA regulation, histone modifications, and chromatin remodelling[(2)]. Histone epigenetic alterations are thought to be a broad area of inquiry for the introduction of novel drug development strategies. Histones are subjected to acetylation and deacetylatio by the opposite action of two enzymes called histone acetyl-transferases (HATs) and histone deacetylases (HDACs)[(3)]. It was discovered that many human illnesses, including cancer and neurological disorders, are partly caused by aberrant epigenetic changes. HDACs are enzymes catalysing the acetyl functional group subtraction from the histone lysine side chain. In humans. eighteen HDAC enzymes were identified which involve either zinc ion or NAD^+ as cofactors[(4)], Based on their similarity to yeast HDACs, eleven of the eighteen HDACs are zinc-dependent and are categorized into Classes I, II, and IV. Class III HDACs are NAD-dependent HDACs and are called the sirtuins[(5)].

HDAC inhibition is correlated with cancer treatment[(6)].

Several HDAC inhibitors including vorinostat, belinostat, romidepsin and panobinostat have been approved by FDA for the treatment of malignancies[7].

Most of the FDA-approved HAD inhibitors lack the selectivity and the penetration of solid tumor[8]. HDAC inhibitors have three main pharmacophoric moieties including, a hydrophobic linker, a zinc-binding group (ZBG), and a protein surface recognition moiety, also known as the "cap" unit. Changing these pharmacophoric moieties is a useful way to introduce more potent and selective agents[9]. The 1,2,4-triazoles derivatives are interesting heteroaromatic motif with a significant bioactivity[10]. This five-membered ring exhibits promising bioisosteric substitution for multiple bioactive moieties. Many compounds under inquiry and experimentation have the 3-amino-1,2,4-triazole core[11]. The aim of this work is to design potential HDAC inhibitors compounds by making modifications to the common pharmacophores of FDA approved HDACi including the replacement of the hydroxamate moiety of vorinostat with heterocyclic 1,2,4-triazole ring as ZBG, inserting a hydrophobic linker, and implantation of diverse cap groups

Materials and Instruments

All starting materials and reagents were provided from commercial sources without further purification. The TLC technique was performed using Merck KGaA TLC silica gel 60 254 sheets of 20*20 “reduced to 3*4cm”. The spot developing was identified by a UV light lamp of 254 nm. The FT-IR spectroscopy analysis was carried out using the FT-IR affinity-1 spectrophotometer (Shimadzu, Japan). Stuart's electric melting point device was utilized to determine the melting point. ^{1}H-NMR analyses were performed using Bruker Avance III, 400 MHz machine implicating *d6* -DMSO as the solvent.

Molecular Docking

Docking studies were performed employing a licensed Glide software embedded within the maestro software from Schrodinger’s modeling company version 13.0135[12]. The reference compound for modeling is vorinostat. The docking process consisted of three main steps; protein preparation, ligand preparation, and grid generation. The crystal structure of Homosapien HDAC6 (PDB ID: 5EDU), HDAC2 (PDB ID: 4LXZ), and HDAC8 (PDB ID: 1T69) proteins was downloaded from protein data bank (PDB)[13-15]Click or tap here to enter text.Click or tap here to enter text.. These proteins were prepared using the protein preparation wizard tool in which bond order was assigned, hydrogens were added, the missing loops of protein were filled, water molecules that are not involved in the interaction (beyond 5 Å from het group) and non-essential atoms were deleted. The second step includes the ligand preparation by Ligperp tool to prepare ligands (**K1-K6**). Finally, ligands were docked with prepared proteins in the grid boundary box with 3-dimension of (10 Å * 10 Å * 10 Å).

ADME study

The pharmacokinetic properties of intestinal absorption, systemic distribution, metabolism, excretion and toxicity can be also identified virtually by ligand based ADME prediction using Qikprobe software in Schrodinger Maestro [16]. From the Qikprobe panel all entries from the project table or workspace from final docking must be chosen, ensuring fast mode selection for ADME analysis and then running QikProp in fast processing mode.

Molecular Dynamic (MD) Simulation

The molecular dynamic (MD) simulation was performed using Desmond module version 2.0 [17], to observe the stability of the ligand in the binding pocket of the protein over a simulation time of 50 nanoseconds (ns). The system was built up by choosing an SPC water model in an orthorhombic periodic box of dimensions of (10 Å*10 Å*10 Å) with OPLS-5 force field, then Na^+ and Cl^- ions were added at neutral pH to neutralize the system then added salts. MD simulations were performed by loading the promising compounds from docking in the MD panel and setting the simulation timing to 50 ns at a temperature of 300 K with a relaxation time of 2 picoseconds (ps) and pressure at 1 bar.

Chemical Synthesis

Synthesis of [4-formyl-N-(1H-1,2,4-triazol-3-yl)benzamide] (Comp. 1)

In a round bottom flask dissolve 4-formylbenzoic acid (6 g, 40 mmol) and 1-ethyl-3-(3-dimethylaminopropyl) carbodiimide (EDC) (9.2 g, 48 mmol) in dichloromethane (DCM) (160 mL), and stirred for 15 min at 0 °C, then added 2-amino-1,2,4-triazole (3.36 g, 40 mmol), 1-hydroxy benzotriazole (HOBt) (0.52 g, 4 mmol), and 4-dimethylaminopyridin (DMAP) (4.8 g, 40 mmol). The mixture was allowed to stir at 0 °C for 2 h, and at room temperature for 18 h. The reaction was monitored by TLC[18Click or tap here to enter text.-20]. After completion, the solvent was removed, and the crude product was extracted from 200 mL of ethyl acetate and 200 mL of distilled water. The organic layer was collected and dried. The collected residue was purified through silica gel column chromatography with ethyl-acetate/ n-hexane (50:50) to obtain compound **1** as a white crystal in 90% yield, m.p. 150-153 °C. FT-IR (ATR; υ, cm^{-1}) 3414 (N-H) stretching of amide, 3008 (C-H) str. of the aromatic ring, 2862, 2762 aldehydes (C-H) str., 1693 aldehyde (C=O) str., 1643 amide (C=O) str., 1543 (C=C) aromatic ring str. ^{1}H-NMR

(400 MHz, DMSO) δ 10.12 (s, 1H), 8.17 (d, *J* = 8.0 Hz, 2H), 8.05 (d, *J* = 8.0 Hz, 2H), 7.81 (s, 2H), 7.66 (s, 1H).

General procedure for the synthesis of compounds (K1-K6)

For each reaction was dissolved compound **1** (1.08 g, 5 mmol) in 15 mL of absolute ethanol, then 5 drops of glacial acetic acid was added gradually to the mixture, followed by the addition of one of the following amines: 4-methoxyaniline (0.615 g, 5 mmol), 2-aminothiazole (0.5 g, 5 mmol), *p*-toluidine (0.50 g, 5 mmol), aniline (0.46 g, 5 mmol), 4-bromoaniline (0.86 g, 5 mmol), naphthylamine (0.71 g, 5 mmol), or phenyl hydrazine (0.54 g, 5 mmol), separately. Each reaction mixture was refluxed for 10-12 h. Upon completion, the mixture for each reaction was transferred into the ice bath for the induction of precipitation. After that the precipitate was washed with cold ethanol, left to dry overnight, and recrystallized from ethanol[21].

(E)-4-((thiazol-2-ylimino)methyl)-N-(1H-1,2,4-triazol-3-yl) benzamide (K1)

Dark yellow crystals, yield 50%, m.p (265-267 ºC). FT-IR (ATR; υ, cm^{-1}) 3190 (N-H) amide stretching, 3074 (C-H) aromatic ring stretching, 1663 (C=O) str. of amide, 1620 (C=N) str. of imine bond, 1562 (C=C) str. of aromatic ring. ^{1}H-NMR (400 MHz, DMSO) δ 9.33 (s, 1H), 8.24 (d, *J* = 8.1 Hz d, 4H), 8.19-8.09 (m, 3H), 7.59 (d, *J* = 3.6 Hz, 1H), 7.32 (d, *J* = 3.6 Hz, 1H).

(E)-4-((phenylimino)methyl)-N-(1H-1,2,4-triazol-3-yl) benzamide (K2)

Yellow crystal, yield 90%, m.p (212) ºC. FT-IR (ATR; υ, cm^{-1}) 3348 (N-H) str. of amide, 3059 (C-H) stretching of the aromatic ring, 1647 (C=O) str.of amide, 1620: (C=N) str. of imine bond, 1597 (C=C) str. of the aromatic ring. ^{1}H-NMR (400 MHz, DMSO) δ 10.42 (s, 1H), 8.74 (s, 1H), 8.10 (s, 3H), 7.46 (t, *J* = 7.5 Hz, 2H), 7.35 (m, 4H), 7.13 (t, *J* = 7.5 Hz, 1H).

(E)-4-((p-tolylimino)methyl)-N-(1H-1,2,4-triazol-3-yl) benzamide (K3)

Yellow crystal, yield 90%, m.p 235 ºC, FT-IR (ATR; υ, cm^{-1}) 3325 (N-H) str. of amide, 3039 (C-H) str. of the aromatic ring, 1647 (C=O) str. of amide, 1624: (C=N) str. of imine bond, 1597 (C=C) str. of the aromatic ring, ^{1}H-NMR (400 MHz, DMSO) δ 10.31 (s, 1H), 8.74 (s, 1H), 8.17 – 8.03 (m, 3H), 7.72 – 7.64 (m, 2H), 7.26 (s, 3H), 7.18 (d, *J* = 8.1 Hz, 2H), 2.34 (s, 3H).

(E)-4-((naphthalen-2-ylimino)methyl)-N-(1H-1,2,4-triazol-3-yl) benzamide (K4)

Brown crystal, yield 50%, m.p range (253-256), FT-IR (ATR; υ, cm^{-1}) 3232 (N-H) str. of amide, 3055 (C-H) str. of aromatic ring, 1643 (C=O) str. of amide, 1616: (C=N) str. of imine bond, 1581 (C=C) str. of aromatic ring. ^{1}H-NMR (400 MHz, DMSO) δ 10.63 (s, 1H), 8.93 (s, 1H), 8.51 (s, 1H), 8.19 (m, 3H), 7.97 (m, 4H), 7.89 (m, 3H), 7.61 (s, 1H), 7.52 (s, 2H).

(E)-4-(((4-bromophenyl)imino)methyl)-N-(1H-1,2,4-triazol-3-yl) benzamide (K5)

Off-white crystal, yield 85%, m.p range (242-245) ºC, FT-IR (ATR; υ, cm^{-1}) 3363 (N-H) str. of amide, 3050 (C-H) str. of aromatic ring, 1651 (C=O) str. of amide, 1627 (C=N) str. of imine bond, 1593 (C=C) str. of aromatic ring. ^{1}H-NMR (400 MHz, DMSO) δ 10.52 (s, 1H), 8.74 (s, 1H), 8.09 (s, 2H), 8.06 (d, *J* = 7.4 Hz, 1H), 7.60 – 7.50 (m, 4H), 7.30 (d, *J* = 8.2 Hz, 2H), 7.13 (d, *J* = 8.2 Hz, 1H).

(E)-4-(((4-methoxyphenyl)imino)methyl)-N-(1H-1,2,4-triazol-3-yl) benzamide (K6)

Yellow crystal, yield 85%, m.p range (240-242) ºC, FT-IR (ATR; υ, cm^{-1}) 3329 (N-H) str. of amide, 3012 (C-H) str. of aromatic ring, 2958 aliphatic (C-H) str., 1647 (C=O) str. of amide, 1620 (C=N) str. of imine bond, 1597 (C=C) str. of aromatic ring. ^{1}H-NMR (400 MHz, DMSO) δ 10.25 (s, 1H), 8.76 (s, 1H), 8.6 (s, 2H), 7.70 (d, 2H), 7.37 (d, 2H), 7.02 (d, 2H), 6.95 (d, 2H), 3.8 (s, 3H).

Biological Studies

Two human cell lines (lung cancer cell A549 and HeLa cell) acquired from the IRAQ Biotech Cell Bank Unit located in Basra and kept in RPMI-1640 supplemented with 100 units/mL of penicillin, 100 µg/mL of streptomycin, and 10% fetal bovine. Trypsin-EDTA was used to passage the cells, which were then reseeded at 70% confluence two to three times per week and cultivated at 37 °C and 5% CO_2[22].

On 96-well plates, the MTT cell viability assay was performed to ascertain the cytotoxic effect. 1×10^4 cells/well were used to seed cell lines[23]. Cells were treated with tested compounds **K1**–**K6**, at concentrations of 10, 5, 2.5, 1.25, 0.62, and 0.31 µg/ml for each compound, after 24 hours or the achievement of a confluent monolayer. Following a 72-hour treatment period, the media was removed, 28 µL of a 2 mg/mL MTT solution was added, and the cells were incubated for 2 hours at 37 °C to determine the viability of the cells. Following the removal of the MTT solution, 100 µL of DMSO was added to the wells to solubilize the residual crystals. The mixture was then incubated for 15 minutes at 37 °C while being stirred[24]. The assay was run in triplicate, and the absorbency was measured using a microplate reader set at the test wavelength of 620 nm. The following formula was used to determine the percentage of cytotoxicity or the inhibition rate of cell growth. Proliferation rate (PR)= B/A∗100 where A is the mean optical density of untreated wells B is the optical density of treated wells and then calculation the rate of inhibition (IR) by equation (IR)=100-PR[25].

Results and Discussion

Molecular Docking Study

The molecular docking study for the designed compounds that established with modification of the main pharmacophores of vorinostat include replacement of hydroxamate moiety in ZBG by heterocyclic ring, modification of the cap group by possible substituent and replacement aliphatic linker by aromatic one to enhance the binding within the active site and increase the docking score. The predicted binding affinity for the designed compounds with various HDAC isoforms was highly promising and it was comparable to vorinostat (Table 1). Docking score helps identify interactions of a ligand with static protein structure, and it has a few approximations and fast calculation. For more accuracy, these results supported by molecular dynamics simulation as both ligand and protein are in motion, and MD simulations is quite close to the in vitro laboratory conditions of biological activity. Most interestingly, the virtual interaction of the most active compound **K5** with HDAC8 (that have best alignment to the protein than vorinostat) shows that the N4 triazole moiety and the amide carbonyl group are forming a bidentate chelation with zinc ion. The amine atom of the amide group forms a hydrogen bonding with Gly151 residue. The linker phenyl moiety is forming π-π stacking with both Phe151 and Phe208. The *p*-bromophenyl cap group is nicely probing outside the active site (Figure 1).

ADME Study

Compounds **K1-K6** were *in-silico* tested for their absorption, distribution, metabolism, and excretion by Qikprobe software within maestro software. The results demonstrated that every examined compound did not violate the Lipinski rule of five to be a drug-like molecule[26]. The final compounds had minimal CNS side effects, good oral absorption, and good gut-blood barrier permeability. Most importantly, compound **K5** involves no metabolically labile moieties in its structure, while vorinostat involves three metabolically labile moieties (Table 2).

Table 1. Docking score of synthetic compounds on various HDACs enzymes

Comp. ID	Docking score		
	HDAC 2 4LXZ in Kcal/mol	**HDAC 6 5EDU in Kcal/mol**	**HDAC 8 1T69 in Kcal/mol**
K1	-8.506	-9.15	-8.54
K2	-8.54	-9.35	-8.47
K3	-8.55	-9.20	-8.46
K4	-8.6	-9.52	-8.32
K5	-6.81	-7.31	-7.62
K6	-8.57	-8.62	-6.77
vorinostat	-7.57	-9.00	-9.107

Table 2. Drug-likeness properties of final compounds

Comp ID	M WT g/mol	Rule of 5	Rule of 3	Oral absorption	Donor HB	AccpHB	#Metab	CNS	QPPCaco nm/sec
K1	335	0	0	3	2	8	1	-2	266.5
K2	291	0	0	3	2	6.5	0	-2	473.6
K3	305	0	0	3	1	5	1	-2	470.9
K4	341	0	0	3	2	6.5	0	-2	471.2
K5	370	0	0	3	2	6.5	0	-2	155.2
K6	321	0	0	3	2	7.25	1	-2	471.5
vorinostat	264	0	0	3	3	6.7	3	-2	138.13

Rule of 3: Number of violations of Jorgensen's rule of three. The three rules are: QPlogS > -5.7, QP PCaco > 22 nm/s, # Primary Metabolites < 7. Compounds with fewer (and preferably no) violations of these rules are more likely to be orally available. CNS: Predicted a central nervous system activity on a –2 (inactive) to +2 (active) scale (software predicted value not log p) .QPPCaco: cell permeability in nm/sec. are a model for the gut-blood barrier for non-active transport. <25 poor, >500 great

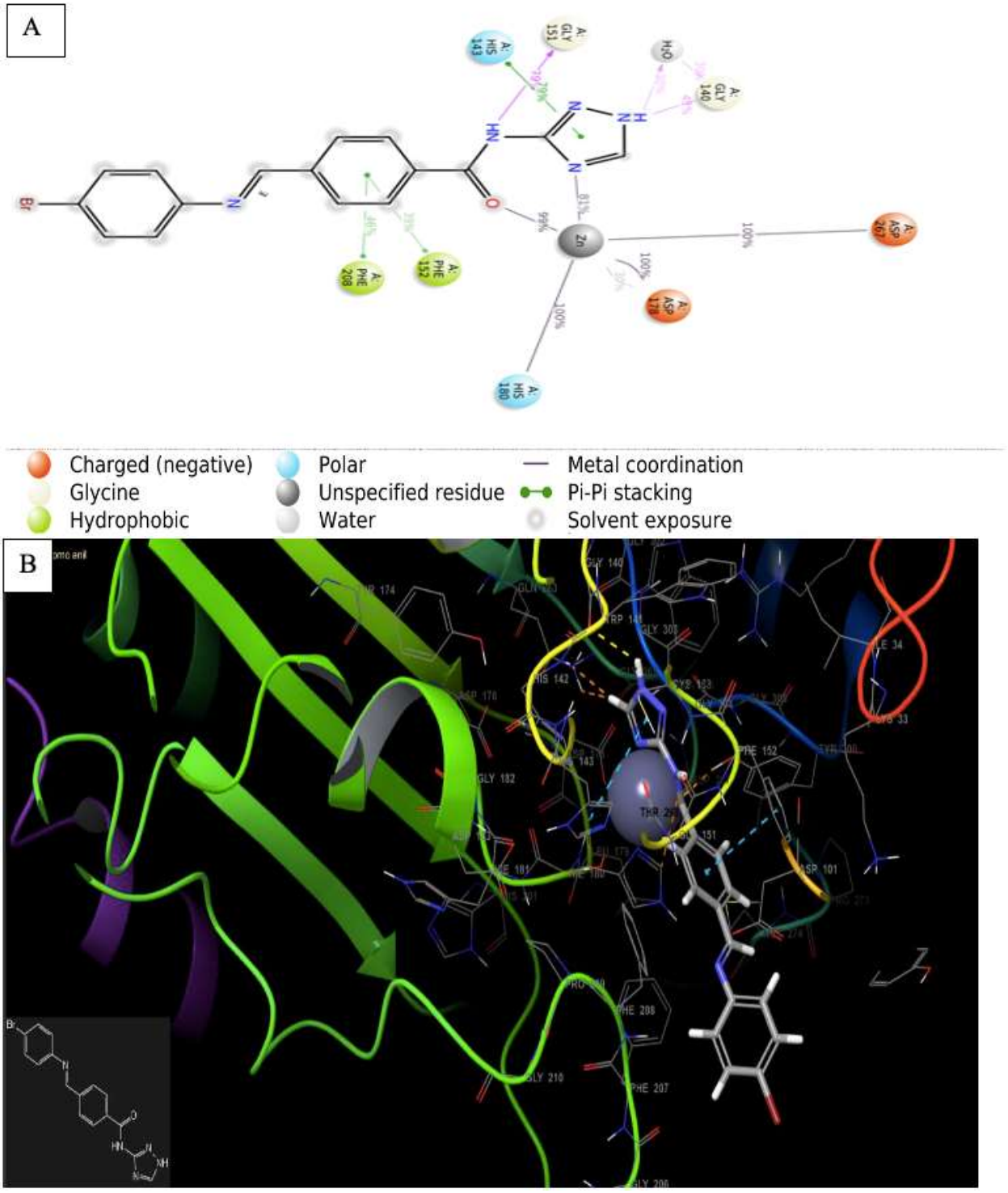

Figure 1. (A) The 2D and (B) 3D interaction diagram of compound K5 with HDAC8 (1T69).

Molecular Dynamics Simulations

In this study, compound **K5** in complex with HDAC8 (1T69) was subjected to MD simulations to understand how compound **K1** interacts with HDAC8 protein when HDAC8 in motion, and to see how long the compound remains stable over simulation time to compare it with MD result of vorinostat. To evaluate the stability of the protein-ligand complex, the RMSD and RMSF measurements were also studied.

Protein-Ligand Root Mean Square Deviation (PL-RMSD).

The result found that compound **K5**-1T69 complex shows more stability profile and best alignment between **K5** and HDAC8 on simulation runs with RMSD value for protein about 1.5 Å (best

value < 3 Å) and for **K5** 2.4-3 Å considered within acceptable range (best value < 2 Å), while for vorinostat, protein RMSD 1.5 Å and vorinostat-RMSD 6 Å (Figure 2).

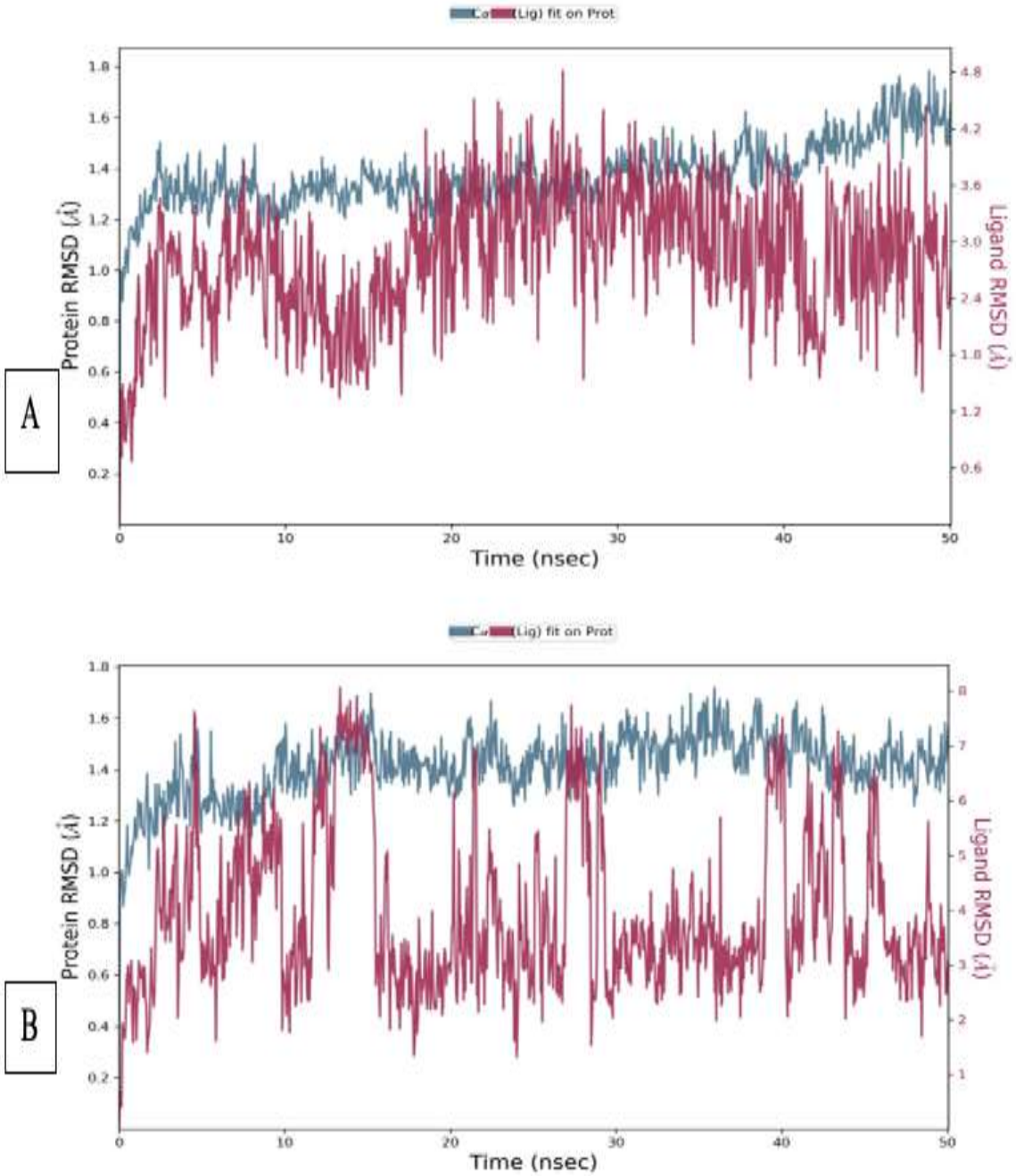

Figure 2. PL-RMSD values in versus time (A) for K5-1T69, (B) for vorinostat-IT69 complex.

Ligand Root Mean Square Fluctuation (L-RMSF)

The Ligand Root Mean Square Fluctuation (L-RMSF) is applied to define the variations in the positions of the ligand's atoms. As seen in figure 3, the compound **K5**-HDAC8 complex initially aligns with the backbone of the protein, and after that, the ligand-heavy atoms' RMSF is determined. The compound **K5** has minimal fluctuation between (1-3 Å) showing that the ligand fits perfectly throughout a simulated time of 23 atoms.

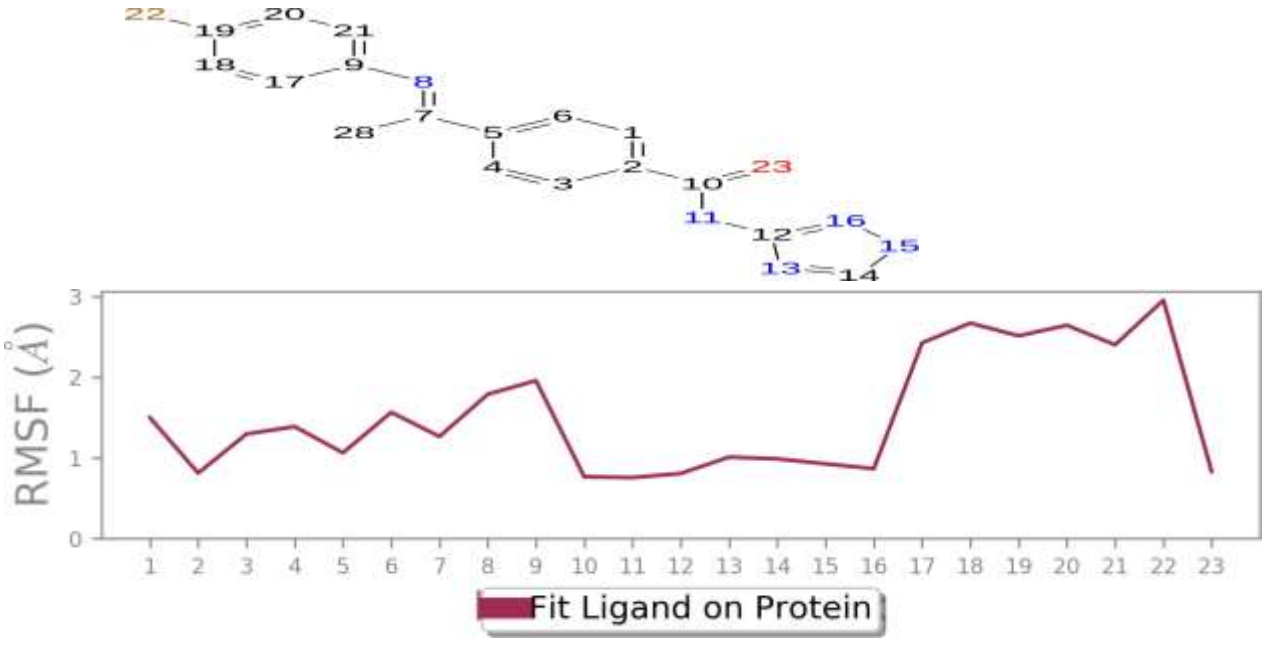

Figure 3. L-RMSF for compound K5-HDAC8 complex.

Chemistry

The synthesis of intermediate **1** [4-formyl-N-(1H-1,2,4-triazol-3-yl)benzamide] was achieved by conducting the amide formation reaction between 4-formylbenzoic acid and 2-amino-1,2,4-triazole in the presence of 1-ethyl-3-(3-dimethylaminopropyl) carbodiimide (EDC), 4-dimethylaminopyridin (DMAP) and 1-hydroxy benzotriazole (HOBt). The mechanism involves the activation of carboxylic acid by EDC through a transfer of a proton from the carboxylic group to form an unstable intermediate that undergoes nucleophilic attack by HOBt to form a reactive ester intermediate[18]. DMAP role as an acyl transferring agent in this coupling reaction is to form a good leaving group intermediate and, at last, a nucleophilic attack of amine on forming intermediate to form the amide. A Schiff base reaction was carried out between the produced aldehyde (intermediate **1)** with variant amines in the presence of a few drops of glacial acetic acid in dry ethanol to synthesize the compounds (*E*)-4-((thiazol-2-ylimino)methyl)-N-(1H-1,2,4-triazol-3-yl) benzamide (**K1**), (*E*)-4-((phenylimino)methyl)-N-(1H-1,2,4-triazol-3-yl) benzamide (**K2**), (*E*)-4-((p-tolylimino)methyl)-N-(1H-1,2,4-triazol-3-yl) benzamide (**K3**), (*E*)-4-((naphthalen-2-ylimino)methyl)-N-(1H-1,2,4-triazol-3-yl) benzamide (**K4**), (*E*)-4-(((4-bromophenyl)imino)methyl)-N-(1H-1,2,4-triazol-3-yl) benzamide (**K5**), and (*E*)-4-(((4-methoxyphenyl)imino)methyl)-N-(1H-1,2,4-triazol-3-yl) benzamide (**K6**) in acceptable yields.

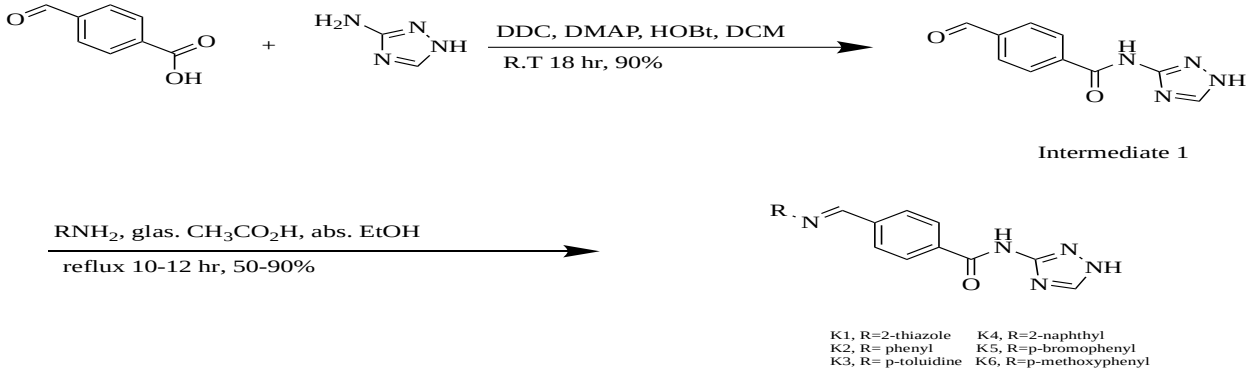

Scheme 1. The synthesis of final compounds.

Antiproliferative Study

Compounds **K1**-**K6** were *in vitro* tested for their antiproliferative activity against A549 and HeLa cancer cell lines to compare their cytotoxic effect with reference standard chemotherapeutic

agents vorinostat[26]. The study started with a single dose test at a concentration of 10 µM against the A549 cell line to identify effective compounds that inhibit cancer cells, then the dose-response study at concentrations (10, 5, 2.5, 1.25, 0.62 and 0.31 µM) was carried out to calculate the IC_{50}. The results show that compound **K5** showed higher antiproliferative activity against A549 lung cancer cells with IC_{50} value (4.4 µM) in comparison with vorinostat (9.5 µM) while compounds **K1**, **K2**, and **K6** have lower cytotoxic effects with IC_{50} of (19.2, 17.6, and 10.6 µM) respectively (Table 3). The cytotoxicity activity against HeLa cancer cells indicated that compounds **K1**, **K2** and **K5** have the highest cytotoxic effect with IC_{50} values for compounds **K1** (4.9 µM), **K2** (5.3 µM) and **K5** (5.3 µM), while the IC_{50} for vorinostat is (8.4 µM). While compound **K6** showed lower cytotoxic activity. The antiproliferative pattern for the final compounds against Hela cells is comparable to the activity of vorinostat. This might be attributed to the high expression of HDAC8 in Hela cells[27,28]. On the other hand, the steric and the electronic properties of the cap group might control the antiproliferative activity against A549 cells, as compound **K5** that involves a *para*-bromo-phenyl substitution showing a superior cytotoxicity activity (Table 3).

Table 3. The IC_{50} values for tested compounds against HeLa cell and lung cancer cell (A549)

Comp. ID	IC_{50} (HeLa cell)	IC_{50} Lung cancer (A549)
K1	4.9	19.2
K2	5.3	17.6
K5	5.3	4.4
K6	--	10.6
vorinostat	8.4	9.5

Conclusion

The modeling tools were applied to successfully design possible new 1,2,4-triazole-based HDAC inhibitors. The designed (**K1–K6**) molecules were successfully synthesized, and their chemical structure was characterized by ^{1}H-NMR and FT-IR analysis. The antiproliferative activity was highly promising as **K1**, **K2** and **K5** showed a superior cell inhibition activity compared to vorinostat, A strong agreement was concluded between the predicted outcomes of the molecular modeling studies and the biological investigation. In contrast to vorinostat, the virtual pharmacokinetic (ADME) studies demonstrated that compound **K5** has no metabolic labiality, minimal CNS side effect, and did not violate the Lipinski rule of five or Jorgensen's rule of three. These results are highly encouraging and might open the avenue for the development of new HDAC inhibitors.

Acknowledgement

We would like to thank the College of Pharmacy, University of Baghdad for all support and help.

Conflict of Interest

The authors declare no conflict of interest.

Funding

The work is partially funded by the College of Pharmacy, University of Baghdad.

Ethics Statement

As a graduate student, I identified the values of respect, honesty, integrity, commitment, and responsibility as their guiding principles. No animal or human studies have been carried out in this work**.**

Author Contribution

Ayad A. Al-Hamashi is contributed in the designing and molecular modeling through the synthesis and testing of synthesized compounds, also writing and arrangements of manuscript. Zaid Mahmood Mohammed performed the design, synthesis, purification, and evaluating the cytotoxicity activity for the final molecules, and writing the manuscript.

Reference

1. Ames BN, Gold LS, Willett WC. The causes and prevention of cancer. Proc Natl Acad Sci U S A. 1995 Jun 6;92(12):5258-65.
2. Cheng, Y., He, C., Wang, M. *et al.* Targeting epigenetic regulators for cancer therapy: mechanisms and advances in clinical trials. *Sig Transduct Target Ther* **4**, 62 (2019).
3. Ali RM, Al-Hamashi AA. Molecular docking, ADMET, molecular dynamic simulation, synthesis, and preliminary antiproliferative study of 1, 2, 4-thiadiazole derivatives as possible histone deacetylase inhibitors. *Tropical Journal of Pharmaceutical Research.* 2024 Jul 1;23(7):1069-76.
4. Al-Hamashi, A., Abdulhadi, S., Ali, R. (2023). Evaluation of Zinc Chelation Ability for Non-Hydroxamic Organic Moieties, *Egyptian Journal of Chemistry*, 66(5), pp. 215-221.
5. Hasan Y, Al-Hamashi A. Identification of Selisistat Derivatives as SIRT1-3 Inhibitors by in Silico Virtual Screening. *Turkish Comput Theor Chem.* 2023 Jul 4;8(2):1–11. Ganai SA, Farooq Z, Banday S, Altaf M. In silico approaches for investigating the binding propensity of apigenin and luteolin against class I HDAC isoforms.

Future Med Chem. 2018 Aug 1;10(16):1925-1945.

6. Al-Hamashi AA, Koranne R, Dlamini S, Alqahtani A, Karaj E, Rashid MS, Knoff JR, Dunworth M, Pflum MKH, Casero RA Jr, Perera L, Taylor WR, Tillekeratne LMV. A new class of cytotoxic agents targets tubulin and disrupts microtubule dynamics. *Bioorg Chem.* 2021 Nov;116:105297.
7. Karagiannis D, Rampias T. HDAC Inhibitors: Dissecting Mechanisms of Action to Counter Tumor Heterogeneity. *Cancers* (Basel). 2021 Jul 16;13(14):3575.
8. Abdulameer AM, Al-Hamashi AA. Docking, ADMET Study, Synthesis and Biological Evaluation of Isoxazole Derivatives as Potential Histone Deacetylase Inhibitors. *History of Medicine.* 2023 Oct 2;9(1):2501-8.
9. Kaur R, Dwivedi AR, Kumar B, Kumar V. Recent Developments on 1,2,4-Triazole Nucleus in Anticancer Compounds: A Review. *Anticancer Agents Med Chem*. 2016;16(4):465-89.
10. Grytsai O, Valiashko O, Penco-Campillo M, Dufies M, Hagege A, Demange L, Martial S, Pagès G, Ronco C, Benhida R. Synthesis and biological evaluation of 3-amino-1,2,4-triazole derivatives as potential anticancer compounds. *Bioorg Chem.* 2020 Nov; 104:104271.
11. Halgren, T. A.; Murphy, R. B.; Friesner, R. A.; Beard, H. S.; Frye, L. L.; Pollard, W. T.; Banks, J. L., "Glide: A new approach for rapid, accurate docking and scoring. 2. Enrichment factors in database screening", *J. Med. Chem.*, 2004, *47*, 1750–1759.
12. Hai, Y., Christianson, D. Histone deacetylase 6 structure and molecular basis of catalysis and inhibition. *Nat Chem Biol* **12**, 741–747 (2016).
13. Lauffer BE, Mintzer R, Fong R, Mukund S, Tam C, Zilberleyb I, Flicke B, Ritscher A, Fedorowicz G, Vallero R, Ortwine DF, Gunzner J, Modrusan Z, Neumann L, Koth CM, Lupardus PJ, Kaminker JS, Heise CE, Steiner P. Histone deacetylase (HDAC) inhibitor kinetic rate constants correlate with cellular histone acetylation but not transcription and cell viability. *J Biol Chem.* 2013 Sep 13;288(37):26926-43.
14. Somoza JR, Skene RJ, Katz BA, Mol C, Ho JD, Jennings AJ, Luong C, Arvai A, Buggy JJ, Chi E, Tang J, Sang BC, Verner E, Wynands R, Leahy EM, Dougan DR, Snell G, Navre M, Knuth MW, Swanson RV, McRee DE, Tari LW. Structural snapshots of human HDAC8 provide insights into the class I histone deacetylases. *Structure*. 2004 Jul;12(7):1325-34.
15. Schrödinger Release 2024-1: QikProp, Schrödinger, LLC, New York, NY, 2024.
16. Bowers, K. J.; Chow, E.; Xu, H.; Dror, R. O.; Eastwood, M. P.; Gregersen, B. A.; Klepeis, J. L.; Kolossvary, I.; Moraes, M. A.; Sacerdoti, F. D.; Salmon, J. K.; Shan, Y.; Shaw, D. E.,Scalable algorithms for molecular dynamics simulations on commodity clusters, *Proceedings of the ACM/IEEE Conference on Supercomputing (SC06), Tampa, Florida*, 2006, November 11-17
17. Ghosh AK, Shahabi D. Synthesis of amide derivatives for electron deficient amines and functionalized carboxylic acids using EDC and DMAP and a catalytic amount of HOBt as the coupling reagents. *Tetrahedron Lett*. 2021 Jan 19;63:152719.
18. Saeed AM, Al-Hamashi AA. Molecular Docking, ADMET Study, Synthesis, Characterization and Preliminary Antiproliferative Activity of Potential Histone Deacetylase Inhibitors with Isoxazole as New Zinc Binding Group. *Iraqi J of Pharm Sci*. 2023 Nov 3;32(Suppl.):188-203.
19. Mosa HM, Al-Hamashi AA. Design, Synthesis, and Cytotoxicity Evaluation of Sulfonamide Derivatives as Potential HDAC Inhibitors. *Azerbaijan Pharmaceutical and Pharmaco-therapy Journal*. 2023;22(2):214-7
20. Hadi, M.K., Rahim, N.A.H.A., Sulaiman, A.T. and Ali, R.M. Synthesis, Characterization and Preliminary Antimicrobial Evaluation of New Schiff bases and Aminothiadiazole Derivatives of N- Substituted Phthalimide. *Research Journal of Pharmacy and Technology*, 2022;*15*(9), pp.3861-3865..
21. Al-Ali, A.A., Alsalami, K.A.S. and Athbi, A. M. (2022). Cytotoxic effects of CeO_2 NPs and β-carotine and their ability to induce apoptosis in human breast normal and cancer cell lines. *Iraqi J of Sci*. V (63): 3.
22. Falih. S M., Al-Saray S. T, Alfaris A. A. and Al-Ali A.A. (2022). The synergistic effect of eucalyptus oil and retinoic acid on human oesophagus cancer cell line SK-GT-4. *Egyptian journal of medical human genetics*, V. 23:70
23. Al-Shammari, A.M.; Al-Ismaeel, W.N.; Al-Ali, A.A.; Hassan, A.A. and Ahmed, A.A. (2019). Enhancement of Oncolytic Activity of Newcastle Disease virus Through Combination with Retinoic Acid Against Digestive System Malignancies. *Molecular Therapy* 27(4S1):126-127.
24. Freshney, R.I. (2010). Culture of animal cells a manual of basic technique and specialized applications sixth edition, Wiley-Blackwell, P732.
25. Pollastri, Michael. (2010). Overview on the Rule of Five. Current protocols in pharmacology / editorial board, S.J. Enna. Chapter 9. Unit 9.12.
26. Alqosaibi AI, Abdel-Ghany S, Al-Mulhim F, Sabit H. Vorinostat enhances the therapeutic potential of Erlotinib via MAPK in lung cancer

cells. *Cancer Treat Res Commun*. 2022; 30:100509.

27. Z.M. Mohammed, A.A.A. Al-Hamashi, Molecular docking, ADMET and molecular dynamics simulation studies for molecules with expected HDAC inhibition activity. *Gomal Journal of Medical Science* 22,2(2024)164-72.

النمذجة الجزيئية وتخليق ودراسة اولية للنشاط السام لنمو الخلايا السرطانية لمشتقات جديدة محتوية على مشتقات ترايازول مع نشاط تثبيطي متوقع لأنزيمات هيستون ديسيتيلاز

زيد محمود محمد*[1]و اياد عبد علي الهماشي[2]

[1]وزارة الصحة ،دائرة صحة بابل، بابل ، العراق

[2]فرع الكيمياء الصيدلانية، كلية الصيدلة، جامعة بغداد،بغداد ، العراق

الخلاصة

يعد استهداف إنزيمات هيستون دياسيتيلاز (HDACs) طريقة فعالة لعلاج مجموعة من الأمراض، بما في ذلك السرطان. تم استخدام بعض مثبطات HDAC سريريًا. معظمها مثبطات غير انتقائية ولها خصائص حركية دوائية ضعيفة. ولذلك، هناك عدة محاولات جارية لتطوير مثبطات جديدة ذات ميزات تركيبية مثالية للتغلب على محدودية الهيكل التركيبي للمركبات الحالية. في هذا العمل، تم اقتراح ست مركبات جديدة تحتوي على حلقة تريازول (**K1-K6**) من خلال تحوير خاص لأجزاء التركيب الجزيئي الشائع لمثبطات HDAC باستخدام (١،٢،٤-تريازول) كمجموعة ربط لعنصر الزنك (ZBG)، ومجاميع متنوعة في مجموعة الغطاء، ورابط. تم دراسة هذه المركبات من خلال دراسة الرسو الجزيئي مع بروتينات HDAC6، HDAC2، وHDAC8. كشفت دراسة الرسو أن المركبات المقترحة لها درجة رسو لمركب **K1** (-٨,٥٤ كيلو كالوري /مول)]، **K2**(-٨,٤٧ كيلو كالوري / مول)، **K3** (-٨,٤٦ كيلو كالوري / مول)، **K4** (-٨,٣٢ كيلو كالوري /مول)، **K5** (-٧,٦٢ كيلو كالوري/مول)]، **K6** (-٦,٧٧ كيلو كالوري /مول)]، وفورينوستات (-٩,١ كيلو كالوري /مول) ضد HDAC8. تم تصنيع المركبات النهائية باستخدام طرق التخليق العضوي التقليدية بدءًا من تكوين رابطة الأميد باستخدام EDCi، وDMAP، وHOBt، وDIPEA، متبوعة بتفاعل قاعدة شف بين الألديهايد الناتج والأمينات المختلفة لإنتاج المركبات النهائية. تمت تنقية جميع المركبات الناتجة باستخدام إعادة البلورة و/أو باستخدام الكروماتوغرافيا العمودية .تم تشخيص التركيب الكيميائي للمركبات الوسيطة والنهائية بواسطة التحليل الطيفي بالأشعة تحت الحمراء والتحليل الطيفي بالرنين المغناطيسي النووي. أظهر اختبار MTT الأولي للمركبات **K1** و**K2** و**K5** نشاطًا مضادًا للتكاثر السرطاني مشابهًا مع فورينوستات ضد خلايا HeLa بقيم IC_{50} للمركب **K1** (4.9 ميكرو مولر) و**K2** (5.3 ميكرو مولر) و**K5** (5.3 ميكرو مولر) بينما كان IC_{50} للفورينوستات (٨,٤ ميكرو مولر). والأمر الأكثر اهمية أن المركب **K5** أظهر نشاطًا مضادًا للتكاثر أعلى ضد خلايا سرطان الرئة A549 بقيمة IC_{50}(4.4 ميكرومولر) مقارنةً بالفورينوستات (٩,٥ ميكرومولر)، في حين أن المركبات الأخرى كانت اقل تأثيرا سميا.

الكلمات المفتاحية: مثبطات HDAC، فورينوستات، الرسو الجزيئي، محاكاة الديناميكية الجزيئية، نشاط مضاد للتكاثر.